Journal of Visualization, Vol. 10, No. 3 (2007)261-270

Regular Paper

Magnetothermal Wind Visualized by Numerical Computation

Akamatsu, M.*[1] and Higano, M.*[2]

*1 Faculty of Engineering, Yamagata University, 4-3-16 Jonan, Yonezawa, Yamagata 992-8510, Japan.
E-mail: akamatsu@yz.yamagata-u.ac.jp
*2 Akita Prefectural University, 84-4 Tsuchiya-Ebinokuchi, Yuri-honjo, Akita 015-0055, Japan.

Received 21 September 2006
Revised 13 April 2007

Abstract : This study describes the numerical evaluation of the transient and steady state characteristics of a magnetothermal wind created by the Kelvin force inside the bore space of a super-conducting magnet. The model system designed to evaluate the present numerical computations is composed of two coaxial circular pipes with open ends. The outer pipe, acting as the cooling pipe, corresponds to the bore space of the super-conducting magnet, while the inner pipe, acting as the heating pipe, is installed inside this bore space. The vertical magnetic gradient generated in the bore space as a source of the Kelvin force was replaced by that generated by the electric current circulating within the circular electric coil. The computed results indicated that the generation direction, the flow rate, and the flow pattern of the magnetothermal wind strongly depended on the position of the circular electric coil. For instance, when the circular electric coil was placed at the lower end of the heating region, the free convection was accelerated by the Kelvin force and an upward magnetothermal wind with a maximum flow rate was created. On the other hand, when the circular electric coil was placed at the upper end of the heating region, the free convection was suppressed by the Kelvin force and a downward magnetothermal wind was created.

Keywords : Magnetothermal Wind, Free Convection, Air, Kelvin Force, Numerical Computation.

1. Introduction

The Kelvin force (Gray et al., 2001) or magnetizing force (Ozoe, 2005) is a body force generated under an inhomogeneous magnetic field. The generation of this force inside the bore space of a super-conducting magnet has produced many interesting phenomena relevant to various fields such as chemistry, biology, and engineering. For instance, Braithwaite et al. (1991) reported the control of thermal convection in a shallow liquid layer with a paramagnetic property heated from below and cooled from above installed inside a super-conducting magnet with a bore space of 0.12 m in diameter. Berry and Geim (1997) succeeded in levitating a frog inside a super-conducting magnet with a bore space of 0.03 m in diameter. Tagami et al. (1999) succeeded in solidifying magnetically levitated water inside a hybrid magnet with a bore space of 0.052 m in diameter. Our interest is that the Kelvin force can be utilized to control the heat transfer rate of a paramagnetic fluid (e.g., Bai et al., 1999; Tagawa et al., 2001; Kaneda et al., 2002) or a diamagnetic fluid (e.g., Kitazawa et al., 2001; Tagawa et al., 2003).

Uetake et al. (2000) demonstrated that a Kelvin force induced a magnetothermal wind from a vertical open pipe which had a heating region installed inside a super-conducting magnet with a bore space of 0.1 m in diameter. They measured the temperature distributions of the magnetothermal wind in the pipe and calculated the average velocity of the magnetothermal wind based on the theory of Hargen-Poiseuille viscous flow.

However, in order to more thoroughly understand magnetothermal wind and to consider its possible engineering applications, a visualization of magnetothermal wind and the elucidation of its transient and steady state characteristics will be needed. In the present study, therefore, numerical computations were performed in reference to the model system upon which the experimental setup of Uetake et al. was based.

2. Governing Equations

Air shows a paramagnetic property since the absolute value of the mass magnetic susceptibility of paramagnetic oxygen gas is about 250 times that of diamagnetic nitrogen gas at room temperature. It is a feature of paramagnetic fluids that their mass magnetic susceptibilities χ are inversely proportional to their absolute temperature, a relation known as Curie's law, as seen in Eq. (1).

$$\chi = \frac{C}{\theta}, \tag{1}$$

where C is the Curie constant and θ is the absolute temperature.

In the following we show the derivation of the momentum equation including Kelvin force with the temperature dependence of the mass magnetic susceptibility of Eq. (1) as an external force term in addition to the buoyant force term. Equation (2) is the Kelvin force acting on electrically non-conducting fluid under an inhomogeneous magnetic field (Bai et al., 1999):

$$\vec{f} = \frac{1}{2}\nabla\left[H^2 \rho \left(\frac{\partial \xi}{\partial \rho} \right)_T \right] - \frac{1}{2} H^2 \nabla \xi, \tag{2}$$

where H is the magnetic field intensity, ρ is the density, and ξ is the magnetic permeability. The magnetic permeability can be expressed as seen in Eq. (3):

$$\xi = \xi_0 (\rho\chi + 1), \tag{3}$$

where ξ_0 is the magnetic permeability in a vacuum. Equation (2) can be rephrased with the magnetic induction $b(=\xi_0 H)$ and Eq. (3) as follows:

$$\vec{f} = \frac{\rho\chi}{2\xi_0}\nabla b^2. \tag{4}$$

Equation (5) is the momentum equation including the Kelvin force of Eq. (4) as an external force:

$$\rho \frac{D\vec{u}}{Dt} = -\nabla p + \mu \nabla^2 \vec{u} + \frac{\rho\chi}{2\xi_0}\nabla b^2 + \rho\vec{g}. \tag{5}$$

At the isothermal state θ_0, there will be no convection. Therefore, Eq. (5) becomes as follows:

$$0 = -\nabla p_0 + \frac{\rho_0 \chi_0}{2\xi_0}\nabla b^2 + \rho_0 \vec{g}. \tag{6}$$

Pressure p can be represented by the summation of p_0 at the isothermal state of the reference temperature and p' at the perturbed state as seen in Eq. (7):

$$p = p_0 + p'. \tag{7}$$

Subtracting Eq. (6) from Eq. (5) gives

$$\rho \frac{D\vec{u}}{Dt} = -\nabla p' + \mu \nabla^2 \vec{u} + \frac{\rho\chi - \rho_0\chi_0}{2\xi_0} \nabla b^2 + (\rho - \rho_0)\vec{g}. \tag{8}$$

By a Taylor expansion around a static state,

$$\rho\chi = \rho_0\chi_0 + \left[\frac{\partial(\rho\chi)}{\partial\theta}\right]_0 (\theta - \theta_0), \tag{9}$$

$$\rho = \rho_0 + \left(\frac{\partial\rho}{\partial\theta}\right)_0 (\theta - \theta_0). \tag{10}$$

Presuming an ideal gas, $p = \rho G\theta$,

$$\frac{\partial\rho}{\partial\theta} = \frac{\partial}{\partial\theta}\left(\frac{p}{G\theta}\right) = -\rho\frac{1}{\theta} = -\rho\beta, \tag{11}$$

where G is the universal gas constant and β is the volumetric coefficient of expansion. From Curie's law as seen in Eq. (1),

$$\frac{\partial(\rho\chi)}{\partial\theta} = \rho\frac{\partial\chi}{\partial\theta} + \chi\frac{\partial\rho}{\partial\theta} = \rho\left(-\frac{C}{\theta^2}\right) - \rho\beta\chi = -2\rho\beta\chi. \tag{12}$$

When Eqs. (9)-(12) are substituted in Eq. (8) with the Boussinesq approximation, we get Eq. (13):

$$\frac{D\vec{u}}{Dt} = -\frac{1}{\rho_0}\nabla p' + v_0\nabla^2\vec{u} - \frac{\beta_0\chi_0}{\xi_0}(\theta - \theta_0)\nabla b^2 - \beta_0(\theta - \theta_0)\vec{g}, \tag{13}$$

where v_0 is the kinematic viscosity. Although the constant physical properties were used in the present numerical computations, the temperature dependence of the mass magnetic susceptibility in the Kelvin force term and that of the density in the buoyant force term were considered. Equation (13) is the final shape of the momentum equation including Kelvin force with the temperature dependence of the mass magnetic susceptibility. The following are the non-dimensionalized governing equations. Equations (14), (15) and (16) are the equation of continuity, the momentum equation with the Kelvin force term and the energy equation.

$$\nabla \cdot \vec{U} = 0. \tag{14}$$

$$\frac{D\vec{U}}{D\tau} = -\nabla P + Pr \cdot \nabla^2\vec{U} - M \cdot Ra \cdot Pr \cdot T \cdot \nabla B^2 + Ra \cdot Pr \cdot T \cdot \begin{pmatrix} 0 \\ 0 \\ 1 \end{pmatrix}. \tag{15}$$

$$\frac{DT}{D\tau} = \nabla^2 T. \tag{16}$$

The distribution of magnetic induction as a source of the Kelvin force was replaced by that generated by the electric current circulating within the circular electric coil and was computed by Biot-Savart's law in Eq. (17):

$$\vec{B} = -\frac{1}{4\pi} \oint \frac{\left(\vec{A} - \vec{R}\right) \times d\vec{A}}{\left|\vec{A} - \vec{R}\right|^3}. \tag{17}$$

The following dimensionless variables were employed in the above dimensionless equations:

$$\begin{aligned} &\tau = \frac{t}{t_0}, \quad \vec{U} = \frac{\vec{u}}{u_0}, \quad P = \frac{p'}{p_0}, \quad \vec{B} = \frac{\vec{b}}{b_0}, \quad \vec{A} = \frac{\vec{a}}{r_0}, \quad \vec{R} = \frac{\vec{r}}{r_0}, \\ &T = \frac{\theta - \theta_c}{\theta_h - \theta_c}, \quad Ra = \frac{g\beta_0 (\theta_h - \theta_c) r_0^3}{\alpha \nu}, \quad Pr = \frac{\nu}{\alpha}, \quad M = \frac{\chi_0 b_0^2}{\xi_0 g r_0}, \end{aligned} \tag{18}$$

where $\vec{a}$ is the position vector on a circular electric coil, $\vec{r}$ is the position vector in the model system, θ_h is the temperature of the heating wall, θ_c is the temperature of the cooling wall, Ra is the Rayleigh number, α is the thermal diffusivity, Pr is the Prandtl number, and M is the ratio of Kelvin force to the gravitational force. The reference values were defined as follows:

$$r_0 = r_{in}, \quad t_0 = \frac{r_0}{u_0}, \quad u_0 = \frac{\alpha}{r_0}, \quad p_0 = \rho_0 u_0^2, \quad b_0 = \frac{\xi_0 i}{r_0}, \tag{19}$$

where r_{in} is the radius of the inner pipe and i is the electric current in the circular electric coil.

3. Model System and Computational Schemes

Figure 1(a) shows our laboratory's helium-free super-conducting magnet whose bore space is 0.1 m in diameter. Uetake et al. (2000) demonstrated that a Kelvin force induced a magnetothermal wind from an open vertical pipe which had a heating region installed inside the bore space of this super-conducting magnet. Therefore, the model system as seen in Fig. 1(b) was considered in reference to their experimental setup. The model system consists of two coaxial circular pipes with open ends. The outer pipe corresponds to the bore space of the super-conducting magnet. The inner pipe corresponds to the heating pipe installed inside this bore space. The outer pipe has a diameter 5 times and a length 5/3 times those of the inner pipe and is cooled isothermally. The central region of the inner pipe is heated isothermally and the other region is thermally insulated. The vertical magnetic gradient generated in the bore space as a source of the Kelvin force was replaced by this one-turn electric coil. The black broken lines with the arrow show a circular electric coil and the electric current circulating within this coil. The coil diameter was set to be 16 times that of the inner pipe. In the present numerical computations, the circular electric coil was placed at seven different axial positions. The distribution of dimensionless magnetic induction in the system was computed by Eq. (17). The computed distribution almost satisfied the continuity of magnetic induction. Figure 1(c) shows a contour plot of $\mathrm{grad}(B_z)^2$ when the circular electric coil was placed at the middle of the heating region Z = (25/50)HZ. The axial component of the gradient of the square of magnetic induction $\mathrm{grad}(B_z)^2$ becomes zero at (R, Z) = (0, 25) and takes a maximum and a minimum value at (R, Z) = (0, 19) and (R, Z) = (0, 31), respectively.

The dimensionless governing equations were numerically solved using a finite difference method. Inertial terms were approximated by the higher-order up-wind scheme called the UTOPIA scheme (Taylor et al., 1981). The other terms were approximated using either a four-order or a second-order central difference method. The calculation algorithm of pressure term was solved using the HSMAC method (Hirt et al., 1975). The present numerical computations were carried out in the two-dimensional system by assuming axial symmetry within a pipe as a first research step. The domain within the model system was divided into small meshes of 100 in the radial direction and 250 in the axial direction at uniform intervals.

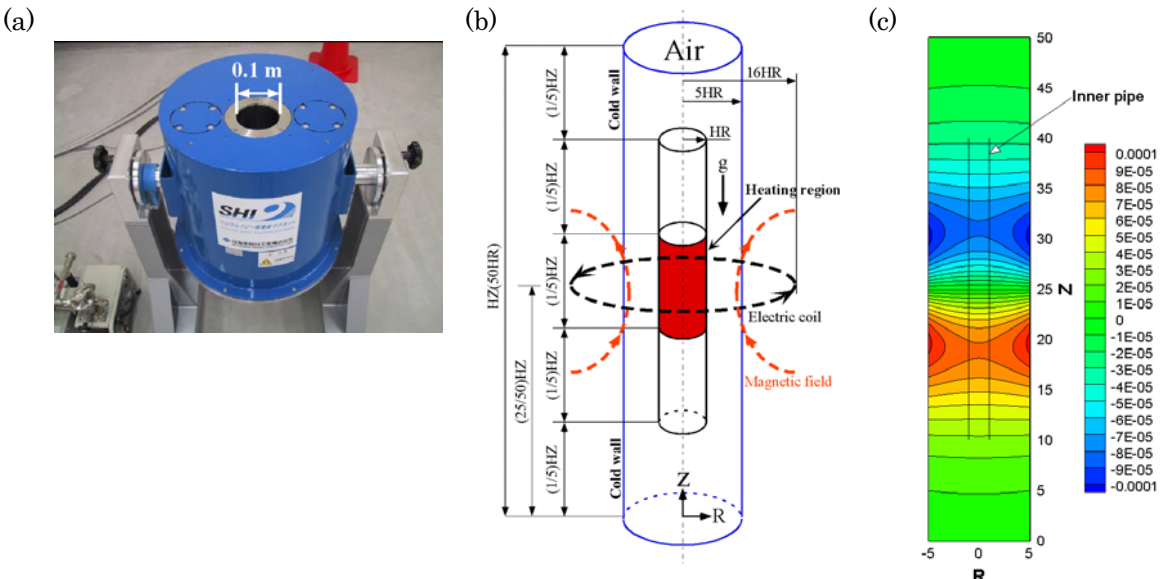

Fig. 1. (a) Helium-free super-conducting magnet. (b) Model system. (c) Contour plot of grad$(B_z)^2$ when the circular electric coil was placed at Z = (25/50) HZ.

The present numerical computations were carried out under the following conditions:

$$
\begin{aligned}
&\textit{Initial conditions:} \quad T = U = W = 0 \quad at \quad \tau = 0, \\
&\textit{Boundary conditions:} \\
&U = \frac{\partial W}{\partial R} = \frac{\partial T}{\partial R} = 0 \quad at \quad R = 0, \quad 0 < Z < HZ, \\
&T = 0, \quad U = W = 0 \quad at \quad R = 5HR, \quad 0 \le Z \le HZ, \\
&\frac{\partial T}{\partial Z} = \frac{\partial U}{\partial Z} = \frac{\partial W}{\partial Z} = 0 \quad at \quad 0 < R < 5HR, \quad Z = 0, HZ, \\
&T = 1, \quad U = W = 0 \quad at \quad R = HR, \quad \frac{2}{5} HZ \le Z \le \frac{3}{5} HZ, \\
&\frac{\partial T}{\partial R} = U = W = 0 \quad at \quad R = HR, \quad \frac{1}{5} HZ \le Z < \frac{2}{5} HZ, \quad \frac{3}{5} HZ < Z \le \frac{4}{5} HZ,
\end{aligned}
\tag{20}
$$

where U , W , and T are the radial velocity, the axial velocity, and the temperature in the dimensionless value, respectively.

4. Computed Results

4.1 Transient Characteristic

Figure 2 shows the transient temperature distribution of the free convection from τ = 0.06 to τ = 0.39 for M = 0, Ra = 5000, and Pr = 0.71. The dimensionless time interval is 0.03. By applying a

thermal gradient, the free convection developed with time, i.e., the high-temperature fluid heated along the heating region of the inner pipe flowed out from the upper open end of the inner pipe due to the effect of the gravitational buoyant force alone.

Figure 3 shows the transient temperature distribution of the upward magnetothermal wind created when the circular electric coil was placed at the lower end of the heating region Z = (20/50) HZ from $\tau = 0.02$ to $\tau = 0.13$ for $M = 2.5 \times 10^5$, $Ra = 5000$, and $Pr = 0.71$. The dimensionless time interval is 0.01. By applying thermal and magnetic gradients, the high-temperature fluid heated along the heating region of the inner pipe was rapidly expelled from the upper open end of the inner pipe, i.e., the upward magnetothermal wind was created by both the Kelvin force and the gravitational buoyant force.

Corresponding figures for the upward magnetothermal wind created when the circular electric coil was placed at the middle of the heating region Z = (25/50) HZ are shown in Fig. 4. By applying thermal and magnetic gradients, the high-temperature fluid heated along the heating region of the inner pipe initially stagnated near the heating region. Subsequently, this stagnated fluid was rapidly expelled from the upper open end of the inner pipe, i.e., again the upward magnetothermal wind was created by both the Kelvin force and the gravitational buoyant force.

Corresponding figures for the downward magnetothermal wind created when the circular electric coil was placed at the upper end of the heating region Z = (30/50) HZ are shown in Fig. 5. By applying thermal and magnetic gradients, the high-temperature fluid heated along the heating region of the inner pipe was rapidly expelled from the lower open end of the inner pipe in spite of the gravitational field, i.e., the downward magnetothermal wind was created by both the Kelvin force and the gravitational buoyant force.

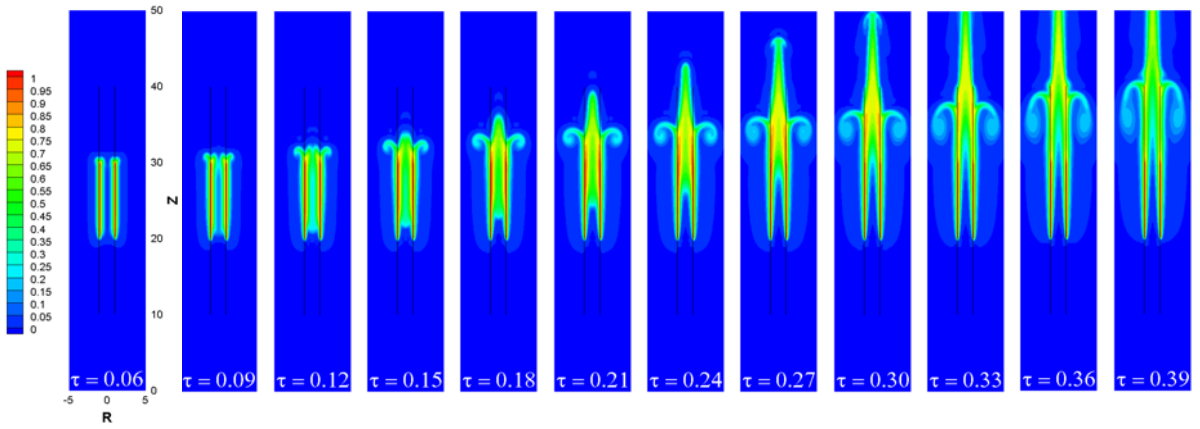

Fig. 2. Transient temperature distribution of the free convection.

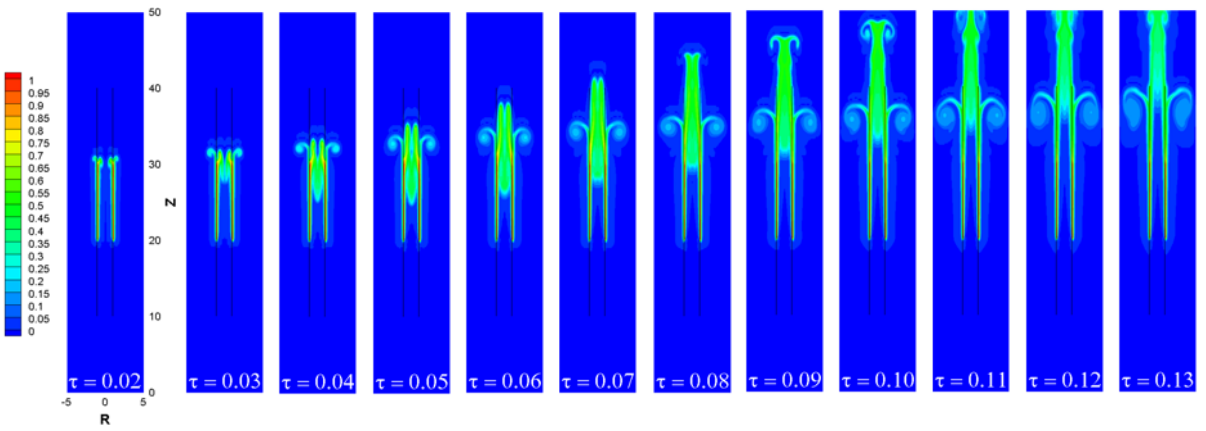

Fig. 3. Transient temperature distribution of the upward magnetothermal wind created when the circular electric coil was placed at Z = (20/50) HZ.

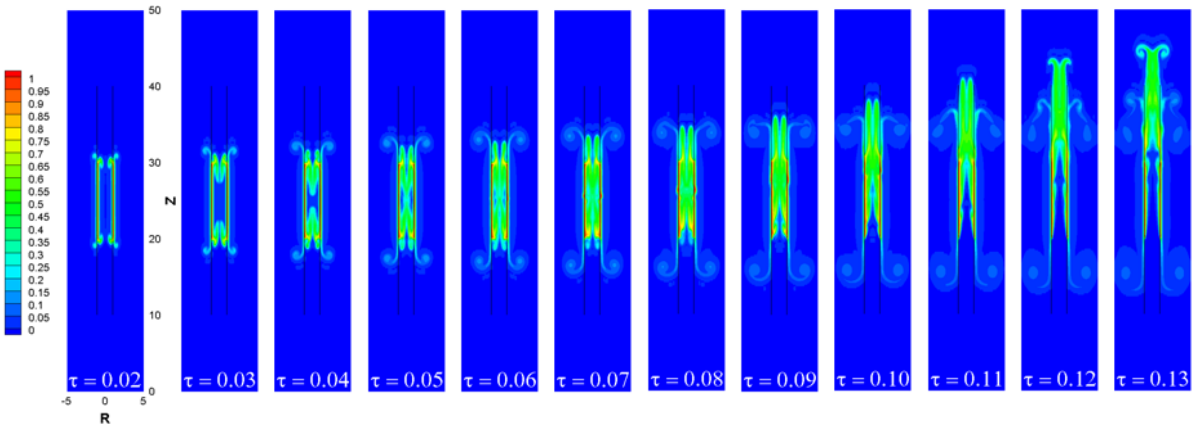

Fig. 4. Transient temperature distribution of the upward magnetothermal wind created when the circular electric coil was placed at Z = (25/50) HZ.

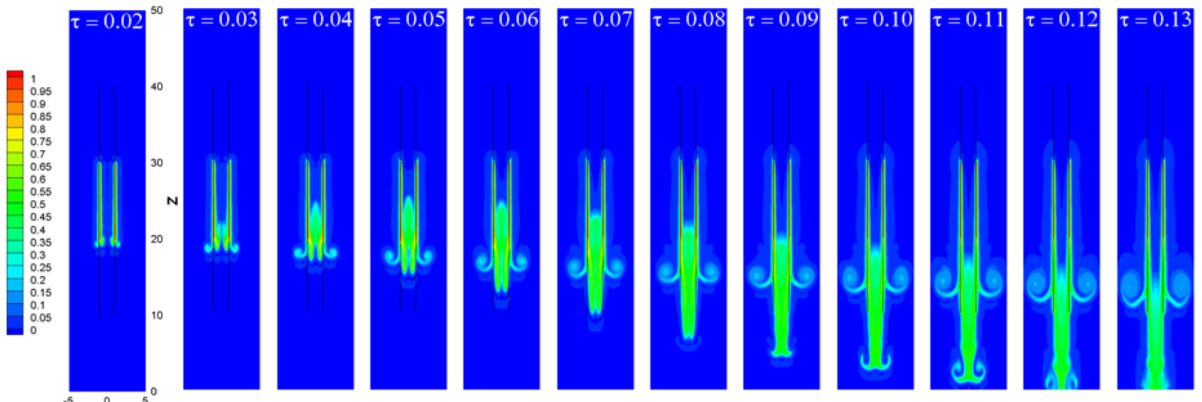

Fig. 5. Transient temperature distribution of the downward magnetothermal wind created when the circular electric coil was placed at Z = (30/50) HZ.

4.2 Steady State Characteristic

Figure 6 shows the temperature distribution and radial profiles of the axial velocity at the ends of the inner pipe at the steady state. Figure 6(a) shows those of the free convection in Fig. 2. Figures 6(b) and 6(c) show those of the upward magnetothermal wind seen in Figs. 3 and 4, respectively. Figure 6(d) shows those of the downward magnetothermal wind seen in Fig. 5. The thermal boundary layer of the magnetothermal wind became thinner than that of free convection since the high-temperature fluid was expelled at the faster speed by the Kelvin force. On the other hand, the axial velocity distribution of the magnetothermal wind showed not a Hargen-Poiseuille viscous flow but two sharp peaks.

Corresponding figures for the magnetothermal wind created when the circular electric coil was placed at other axial positions are shown in Fig. 7. Figures 6(a) and 6(b) show those of the upward magnetothermal wind created when the circular electric coil was placed at Z = (10/50) HZ and Z = (15/50) HZ below the lower end of the heating region, respectively. Figures 6(c) and 6(d) show those of the downward magnetothermal wind created when the circular electric coil was placed at Z = (35/50) HZ and Z = (40/50) HZ above the upper end of the heating region, respectively. The magnetothermal wind created by the Kelvin force gradually weakened as the circular electric coil receded from the heating region.

Figure 8 shows the flow rate at the ends of the inner pipe at the steady state for the magnetothermal wind created by the Kelvin force. It is confirmed that the flow rate balance in the system is maintained. The closed circle shows that of the magnetothermal wind seen in Figs. 6 and 7

for M = 2.5×10^5, Ra = 5000, and Pr = 0.71. The open circle shows that of the magnetothermal wind for M = 2.5×10^5, Ra = 2500, and Pr = 0.71. The flow rate of the upward magnetothermal wind seen in Fig. 6(b) became 3.1 times that of the free convection seen in Fig. 6(a) and 1.4 times that of the upward magnetothermal wind created when the circular electric coil was placed at Z = (20/50) HZ for M = 2.5×10^5, Ra = 2500, and Pr = 0.71. It is considered that the critical axial position of the circular electric coil for creating the downward magnetothermal wind exists between Z = (25/50) HZ and Z = (30/50) HZ under the present numerical conditions.

When the radius of the inner pipe is r_{in} = 0.01 m, the dimensional equivalence for air at 0.1013 MPa and 300 K with χ_0 = 3.09 × 10^{-7} m^3/kg is $(b_z)_{max}$ = 9.87 T on the centerline for M = 2.5 × 10^5 and the maximum temperature difference is 53.5 K for Ra = 5000 and 26.8 K for Ra = 2500. The reference value u_0 is about 2.2 × 10^{-3} m/s. Therefore, the dimensional axial velocity of W = 500 corresponds to 1.1 m/s. The reference value t_0 is about 4.5 s. Therefore, the dimensional time of τ = 0.01 corresponds to 0.045 s.

At present, the experiment is carried out applying our laboratory's helium-free super-conducting magnet seen in Fig. 1(a) in order to prove these numerical results.

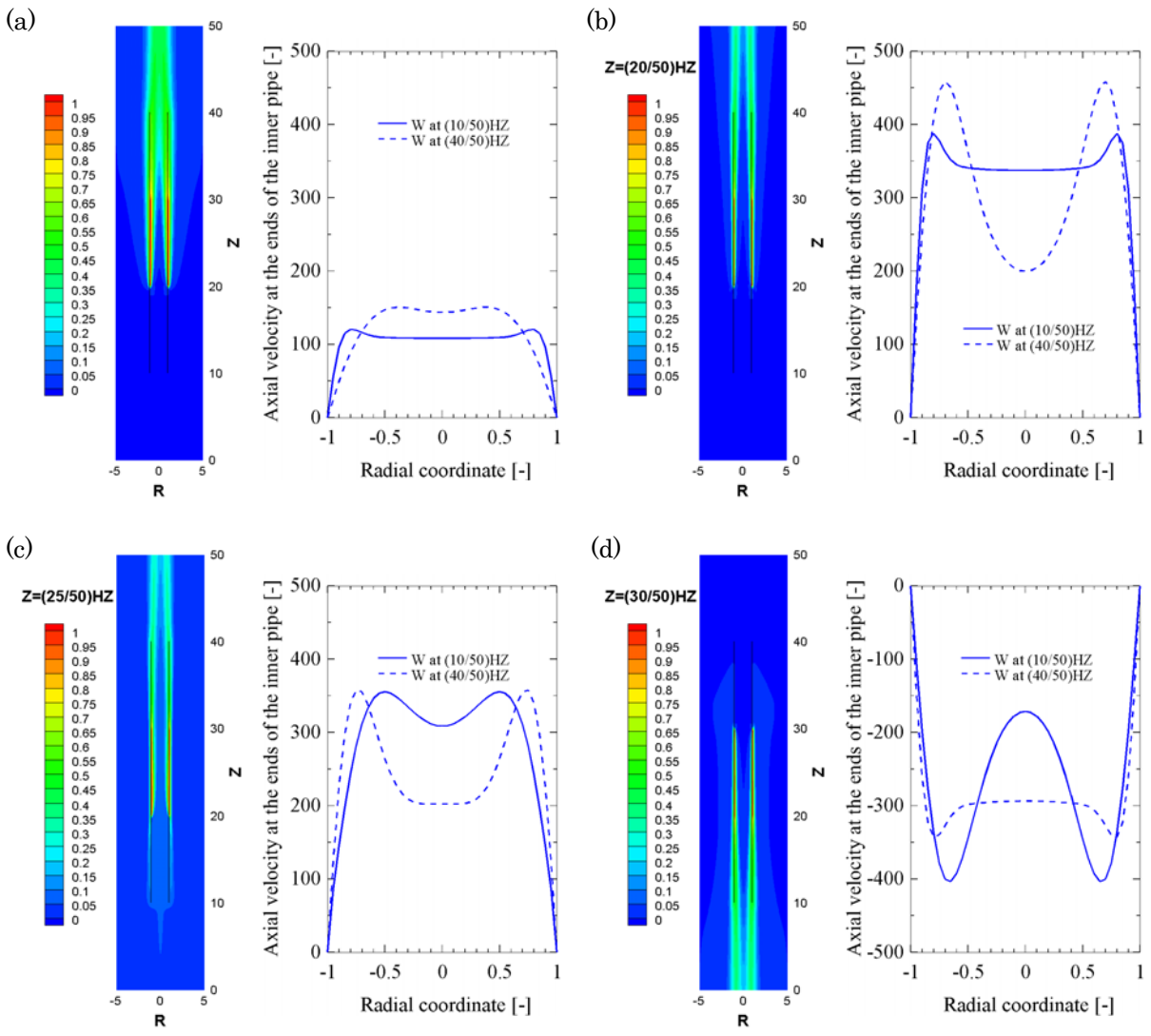

Fig. 6. Temperature distribution and radial profiles of the axial velocity at the ends of the inner pipe at the steady state. (a) Free convection in Fig. 2; (b) Upward magnetothermal wind in Fig. 3; (c) Upward magnetothermal wind in Fig. 4; (d) Downward magnetothermal wind in Fig. 5.

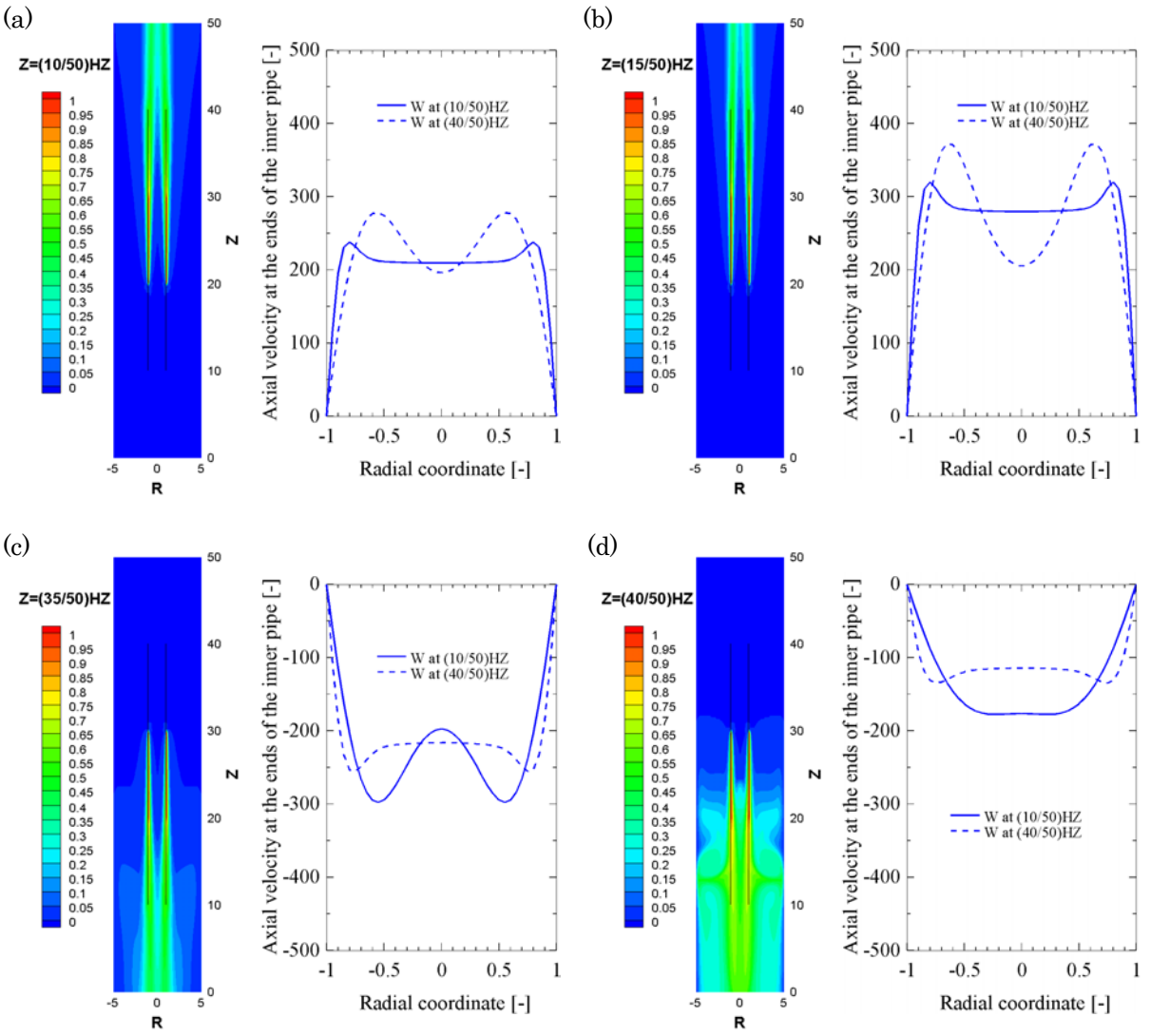

Fig. 7. Temperature distribution and radial profile of the axial velocity at the ends of the inner pipe at the steady state for the upward or downward magnetothermal wind created when the circular electric coil was placed at (a) Z = (10/50) HZ, (b) Z = (15/50) HZ, (c) Z = (35/50) HZ, and (d) Z = (40/50) HZ.

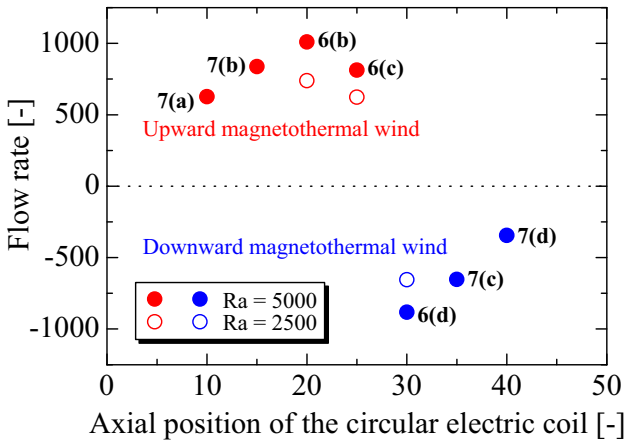

Fig. 8. The flow rate at the ends of the inner pipe at the steady state for the magnetothermal wind created by the Kelvin force.

5. Conclusion

In order to clarify the flow characteristic of the magnetothermal wind created by the Kelvin force inside the bore space of the super-conducting magnet and to consider its possible engineering applications, its visualization was performed by means of numerical computations.

The mass magnetic susceptibility of a paramagnetic gas such as air is inversely proportional to its absolute temperature. Therefore, the Kelvin force works on a high-temperature fluid with a small mass magnetic susceptibility as the repulsive force. On the other hand, the Kelvin force works on a low-temperature fluid with a large mass magnetic susceptibility as the attractive force.

When the circular electric coil is placed at the middle of the heating region or below the middle of the heating region, an upward magnetothermal wind is created by the Kelvin force. On the other hand, when the circular electric coil is placed above the middle of the heating region, a downward magnetothermal wind is created by the Kelvin force.

References

Bai, B., Yabe, A., Qi, J. and Wakayama, N. I., Quantitative Analysis of Air Convection Caused by Magnetic-Fluid Coupling, AIAA Journal, 37 (1999), 1538-1543.

Berry, M. V. and Geim, A. K., Of Flying Frogs and Levitrons, European Journal of Physics, 18 (1997), 307-313.

Braithwaite, D., Beaugnon, E. and Tournier, R., Magnetically Controlled Convection in a Paramagnetic Fluid, Nature, 354 (1991), 134-136.

Gray, D. D., Huang, J. and Edwards, B. F., Two-Dimensional Magnetothermal Plumes, International Journal of Engineering Science, 39 (2001), 1837-1861.

Hirt, C. W., Nichols, B. D. and Romero, N. C., SOLA-A Numerical Solution Algorithm for Transient Fluid Flows, Los Alamos Scientific Laboratory report, (1975), LA-5852.

Kaneda, M., Tagawa, T. and Ozoe, H., Convection Induced by a Cusp-Shaped Magnetic Field for Air in a Cube Heated From Above and Cooled From Below, Journal of Heat Transfer, 124 (2002), 17-25.

Kitazawa, K., Ikezoe, Y., Uetake, H. and Hirota N., Magnetic Field Effects on Water, Air and Powders, Physica B, 294-295 (2001), 709-714.

Ozoe, H., Magnetic Convection, (2005), 139-203, Imperial College Press, London.

Tagami, M., Hamai, M., Mogi, I., Watanabe, K. and Motokawa, M., Solidification of Levitating Water in a Gradient Strong Magnetic Field, Journal of Crystal Growth, 203 (1999), 594-598.

Tagawa, T., Ozoe, H., Inoue, K., Ito, M., Sassa, K. and Asai, S., Transient Characteristics of Convection and Diffusion of Oxygen Gas in an Open Vertical Cylinder under Magnetizing and Gravitational Forces, Chemical Engineering Science, 56 (2001), 4217-4223.

Tagawa, T., Ujihara, A. and Ozoe, H., Numerical Computation for Rayleigh-Benard Convection of Water in a Magnetic Field, International Journal of Heat and Mass Transfer, 46 (2003), 4097-4104.

Taylor, C. and Morgan, K., Computational Techniques in Transient and Turbulent Flow, 2 (1981), 1-35, Pineridge Press, U.K.

Uetake, H., Hirota, N., Nakagawa, J., Ikezoe, Y. and Kitazawa, K., Thermal Convection Control by Gradient Magnetic Field, Journal of Applied Physics, 87 (2000), 6310-6312.

Author Profiles

Masato Akamatsu: He graduated from Kyushu Institute of Technology with a major in Mechanical Engineering in 1994 and received his Dr. Eng. from Kyushu University in 1999. He worked in the Department of Mechanical Engineering, Oita University as a research associate in 1999. Then, he worked in the Department of Machine Intelligence and Systems Engineering, Akita Prefectural University as a research associate since 2000. He has worked in the Department of Mechanical Systems Engineering, Yamagata University as an associate professor since 2007. He has been engaged in the study of thermal convection control of fluids with and without the electric conductivity by a magnetic field.

Mitsuo Higano: He received his M. Eng. in Mechanical Engineering in 1970 from Tohoku University. He also received his Dr. Eng. in Mechanical Engineering in 1994 from Tohoku University. After obtaining his M. Eng., he worked at the Institute of Fluid Science (later renamed the Institute of High Speed Mechanics), Tohoku University as a research associate. He became an associate professor in the Department of Machine Intelligence and Systems Engineering, Akita Prefectural University in 1999, and is currently a professor in the Science and Technology Integration Center. His research interests include Quantitative Visualization, Computational Heat Transfer and Fluid Mechanics, and the Thermophysical Property of Matter.